The Role of Banana Peel Surface Pores through Increasing Temperature for Efficient Hydrogen Production

Abid Fahreza Alphanoda[1*], Erlanda Augupta Pane[1], Agus Riyanto[1], Avita Ayu Permanasari[2]

[1]*Department of Mechanical Engineering, Pancasila University, Jl. Lenteng Agung Raya 56 Jakarta Selatan, 12630, DKI Jakarta, Indonesia.*
[2]*Department of Mechanical and Industrial Engineering, Universitas Negeri malang, Jl. Semarang 5, Malang, East Java, Indonesia.*
**Corresponding author:abid_fahreza@univpancasila.ac.id*

Article history:
Received: 25 September 2024 / Received in revised form: 30 October 2024 / Accepted: 6 November 2024
Available online 14 November 2024

ABSTRACT

Porous carbon derived from banana peel has been synthesized by increasing the temperature range variation from 180 ºC - 270 ºC. The prepared carbon was tested in an experiment using double-chamber photoelectrochemistry to see the results of hydrogen production. SEM-EDX, FTIR, and TGA analyses identified all banana peel carbons. Optical and electrochemical properties were analyzed and measured by UV-Vis, Tauc Relationship, and Pearson Absolute Electronegativity. The amount of hydrogen gas produced from the simulation of UV-A visible light irradiation on variations of BP-240, BP-210, BP-180, and BP-Natural. The surface of BP-270 has more pores and can produce the most significant hydrogen of 1566.05 $\mu mol \cdot g^{-1}$. The data is compared to the weight loss percentage at a temperature of 400 ºC. Generally, the degradation of the weight percentage in banana peel is up to a temperature of 900ºC. This value shows that the most significant energy is needed, 1709190.45 Joules, equivalent to 1.0667×10^{25} eV. At the same time, the energy provided by UV-A is 3.099 eV, equivalent to 4.9661×10^{-19} Joule. Based on the average pores formed by the method used in this study, it explains that the temperature at BP-270 has been able to produce hydrogen in the UV-A exotherm. The increase in banana peel carbon pores increases the separation between electrons and holes and reduces the band gap distance. This study designs an efficient, cheap, and environmentally friendly photoelectrochemical system with waste materials to provide alternative energy sources by utilizing visible light energy.

Keywords: *Banana peel, carbon, hydrogen, photoelectrochemical*

I. Introduction

Fossil fuels, including coal, oil, and natural gas, have become the main source of global energy post-industrial revolution. However, its non-renewable nature and environmental pollution problems, particularly carbon emissions, have made it incompatible with sustainable development goals [1]. Therefore, many countries prioritize alternative energy, one of which is hydrogen [2]. The rational and efficient use of hydrogen energy is one of the best ways to overcome the primary energy crisis. Lately, biomass has been considered a promising source of renewable energy and has attracted much attention. Biomass can be converted into biochar, bio-oil, and syngas through thermochemical conversion, such as pyrolysis [3]. Biochar, especially, can be activated and modified into functional carbon materials, and further used in many fields such as energy, environment, and materials.

The increase in population that occurred in the last 100 years, from 2.2 billion to 8 billion, triggered an increase in food demand, as several factors, such as failures in

DOI: 10.17977/um016v8i22024p421

distribution, led to waste [4]. However diverse these residues are, as long as they contain fermentable sugars, they can be used as raw materials for biochar production. Bananas (Musa sp.), for example, have about 35% of their total weight represented by their peel and, since they are one of the most produced crops in the world, about 100 million tons in 2019, contribute significantly to the production of discarded agroindustrial waste [5]. Therefore, it is important to present solutions or alternatives to utilize this waste, as shown in this study. The biochar formed from banana peels has a lignocellulose matrix, which is mostly composed of lignin (31.6%), cellulose (20.7%), and hemicellulose (17.3%) [6]. Because of this matrix, pretreatment is allowed before the transition to transform the complex structure into sugar monomers for the subsequent conversion of these compounds.

Photocatalysis of hydrogen production absorbs light radiation on a photocatalyst to break hydrogen bonds and covalent bonds in H_2O. The hydrogen breakdown process cannot be separated from the role of the photocatalyst. Photocatalysts in previous studies have discussed the effectiveness of nanoparticles of Zn(O, S) mixed with banana peel biochar. The combination scheme is a way to get low cost in enhancing photocarrier separation because the active carbon sites on the surface of Zn(O, S) attract electrons for hydrogen reduction [7]. Another scheme is maximizing Fe_3O_4 in the oxidation-reduction reaction in water by adding activated carbon banana leaves [8]. However, there has yet to be research on the profile of biochar, or bioactivated carbon from waste in hydrogen production.

Using lignocellulosic residues from organic waste to increase biomass value depends on various methodologies for converting polysaccharides into monomers, which are then converted into ethanol and biochar. Usually, pretreatment and hydrolysis steps with increased temperature are carried out for the production of biochar from lignocellulose biomass. Many applications for hydrogen production use biochar, such as photocatalytic, solar cell devices, and photoelectrochemistry [9]-[11]. Although the bandgap of organic materials has two or more peaks, further processing into biochar is able to absorb light illumination to be active in surface redox reactions such as hydrogen evolution reaction (HER) [12].

Banana peel (BP) is converted into biochar with simple preparation in the form of temperature variations to increase the yield of hydrogen generation. The formation of pores on the surface of BP biochar helps the oxidation efficiency in the water, making it easier to reduce water to hydrogen gas. Double-chamber photoelectrochemical systems are designed to support easy processes and large-scale industrial applications.

II. Material and Methods

1. Material

Banana waste is collected in all canteens around the Pancasila University Campus. Banana peels of the Musa acuminata Cavendish subgroup type are cut into small sizes and then dried in the oven (110 °C), ground in a knife grinder until they reach a particle size of 20 mesh, and stored (−20 °C) until used. Pellets-shaped KOH catalysts are obtained from Sigma Aldrich in Indonesia with a purity of ≥85%.

2. Photoelectrochemical Experiment and Banana Peel Activation

Heat treatment on banana peel with temperature variations of 180 ^oC, 210 ^oC, 240 ^oC, and 270 ^oC for 3 hours. Banana peel with hydrothermal natural room temperature treatment of 30 ^oC was determined to obtain the control variable [13]. Furthermore, Banana Peel was named BP-180, BP-210, BP-240, BP-270, and BP-Original. Adding 50% KOH to BP-180,

BP-210, BP-240, and BP-270 will help activate banana peel into hydrochar [14]. The product is washed using water and ethanol and then dried at room temperature using a hydrothermal process [15]. The selection of the experimental method followed the previous research using a photoelectrochemical double chamber with 15-W UV-A lamp irradiation in the radiation range of 315 - 400 nm [16]. Hydrogen measurements were made using an MQ-8 sensor and recorded through an analog-to-digital converter using an Arduino Uno and recorded with a PC. Hydrogen production testing was carried out by comparing BP-180, BP-210, BP-240, BP-270, and BP-Original for 14400 seconds. The flow of the experiment process can be seen in Figure 1.

Fig. 1. Experimental treatment and testing process.

3. Material Characteristics

The morphological characteristics of banana peels with temperature variations were evaluated using Scanning Electron Microscope (SEM) with type FEI Inspect S50 with Energy Dispersive X-ray (EDX) in Indonesia. The FEI Inspect S50 testing tool with Energy Dispersive X-ray (EDX) can produce an image when electrons interact with a sample. Then, it will get electron backscattering to form a surface image of the sample down to a micron depth. The functional clusters in banana peel were analyzed with IR-Prestige 21, a Fourier transform infrared/FTIR (Shimadzu, Japan). FTIR testing measures the range of wavelengths in the infrared region absorbed by a material. This condition is achieved through the application of infrared radiation to the material sample. Measurement of UV-Vis diffusion reflectance was performed on the UV-vis diffuse reflectance spectrum in the 200-800 nm range (Specord 200 Plus Analytic Jena UV-Vis spectrophotometer) in Indonesia.

4. Thermogravimetric Analysis

In Indonesia, TGA was performed on banana peel samples using a simultaneous thermal analyzer (STA PT 1600, Linseis). In all experiments, the carrier gas was nitrogen (99.99% purity) at a constant flow rate of 100 mL/min to maintain an inert atmosphere and clean up volatile substances resulting from heating. 15 mg of banana peel samples are evenly poured into a platinum container and heated from ambient temperature to 900 °C at a constant heating rate. Each experiment was run in triplicates.

III. Results and Discussions

1. SEM-EDX Results

The results of the BP SEM test are seen in Figure 2. In Figure 2(a). The morphology of BP-180 with a temperature treatment of 180^{o}C is seen. Treatment of BP-210, BP-240, BP-

270 at an increase in temperature of 210 ^{o}C, 240 ^{o}C, and 270 ^{o}C, is seen in Figure 2(b), (c), (d), and (e). The increase in temperature at BP is in line with the formation of porous surfaces [17]. The pores indicate that there is oxide on the surface. Oxides on surfaces tend to have negative values, as evidenced by 3D Surface Plot testing using the ImageJ application. It is proven that as the temperature increases, the Valley area has more and more negative values. This is proven in BP-180, BP-210, BP-240, and BP-270, respectively, in Figure 3(a), (b), (c), (d), and (e).

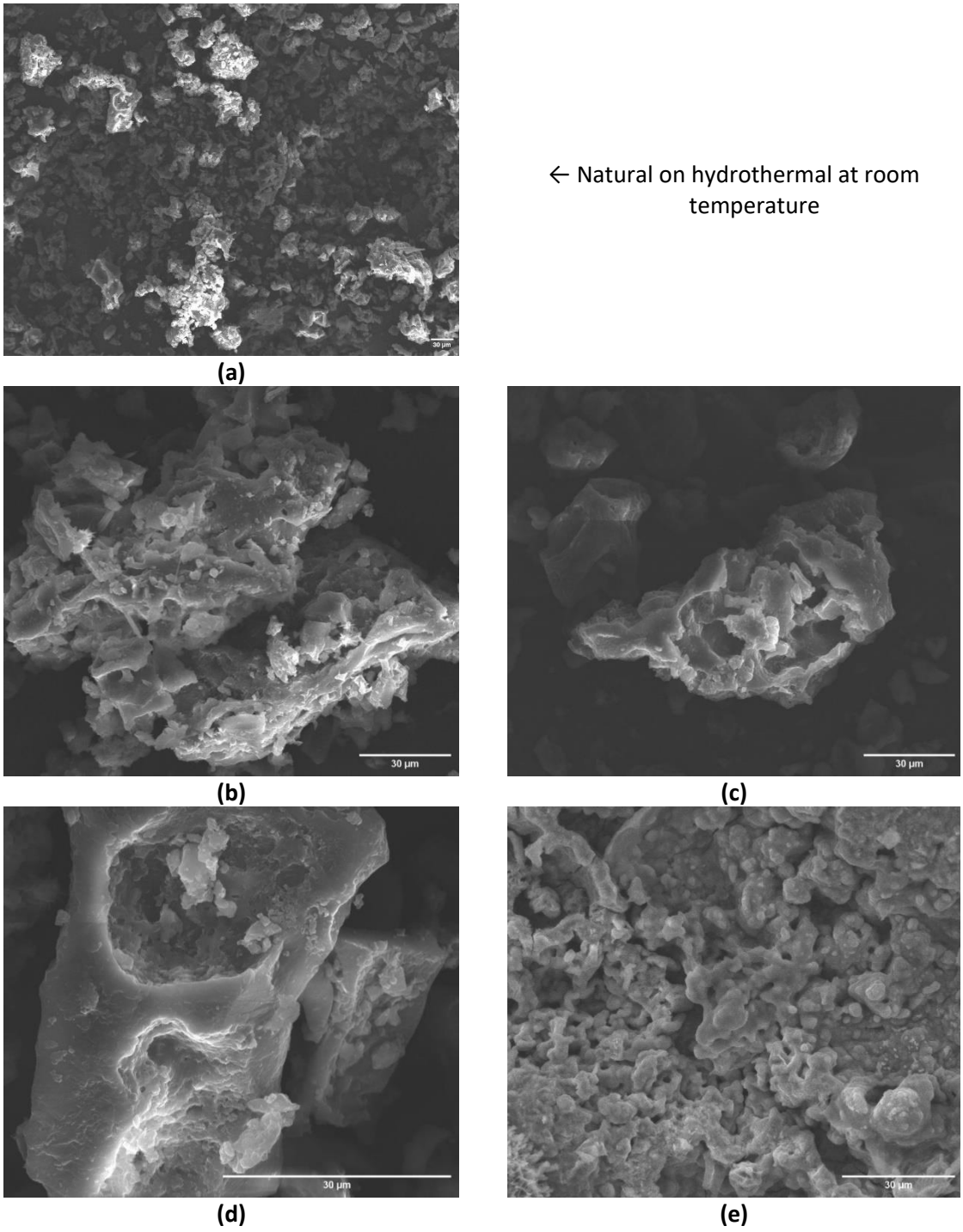

Fig. 2. The results SEM (a) BP-Natural (b) BP-180, (c) BP-210, (d) BP-240, and (e) BP-270.

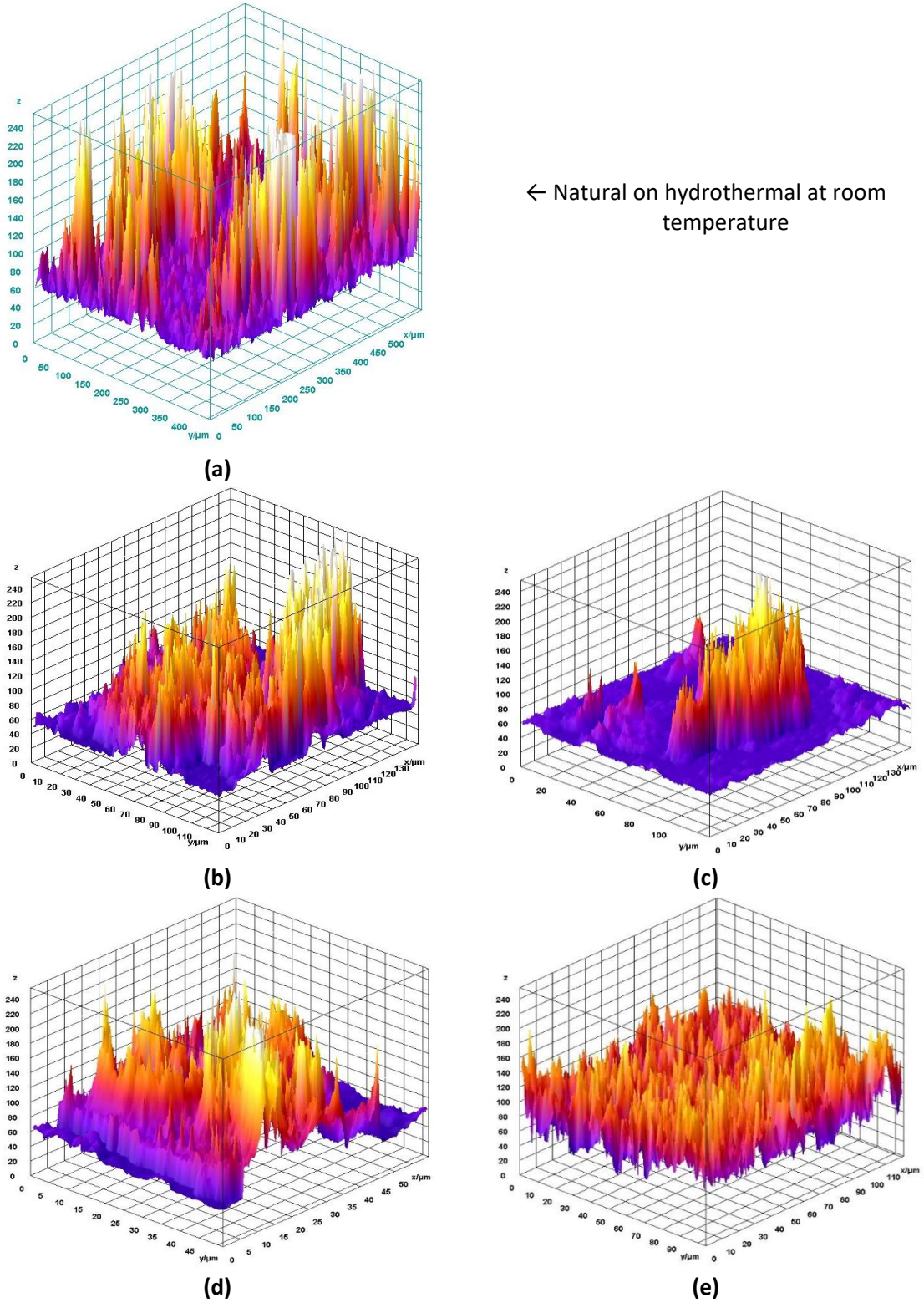

Fig. 3. 3D surface plot with ImageJ (a) BP-Natural (b) BP-180, (c) BP-210, (d) BP-240, and (e) BP-270.

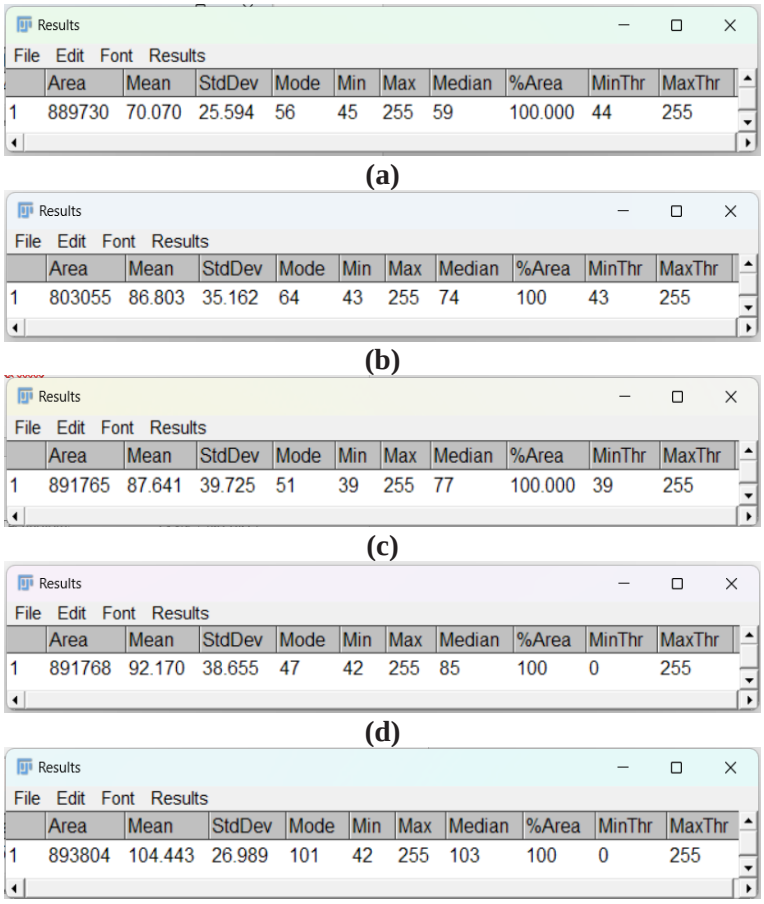

Fig. 4. Plot Results pore surface with ImageJ (a) BP-Natural (b) BP-180, (c) BP-210, (d) BP-240, and (e) BP-270.

Table 1. EDX test results

Chemical Weight %	Banana Peel (BP)
C	75.45
O	12.15
K	1.92
Si	10.48
Chemical Atomic %	
C	75.53
O	11.85
K	1.87
Si	10.75

Based on the SEM data, it was then calculated using ImageJ with the Threshold feature, to obtain the minimum, maximum, and mean pore formation sizes. As seen in Figure 4, measurements were taken on 100% of the entire SEM area. In Figure 4. (a). BP-Natural can be seen getting the smallest pore size of 45 µm, the largest at 255 µm, and the mean pore formation of 70.070 µm. In Figure 4. (b). BP-180 can be seen getting the smallest pore size of 43 µm, the largest at 255 µm, and the mean pore formation of 86.803 µm. In Figure 4.

(c). BP-210 can be seen getting the smallest pore size of 39 µm, the largest at 255 µm, and the mean pore formation of 87.641 µm. In Figure 4. (d). It can be seen that BP-240 has the smallest pore of 42 µm, the largest of 255 µm, and the mean pore formation of 92.170 µm. In Figure 4. (e). It can be seen that BP-270 has the smallest pore of 42 µm, the largest of 255 µm, and the mean pore formation of 104.443 µm. These results indicate that the pores formed are still in the macropore phase, but increasing the temperature is proven to increase the uniformity of pore formation in the banana peel. The EDX results in Table 1 show that carbon has the largest atomic content, 75.53%, in banana peel. The presence of oxygen atoms in the EDX results strengthens the presence of oxide molecules in banana peel, in line with the formation of pores on the surface.

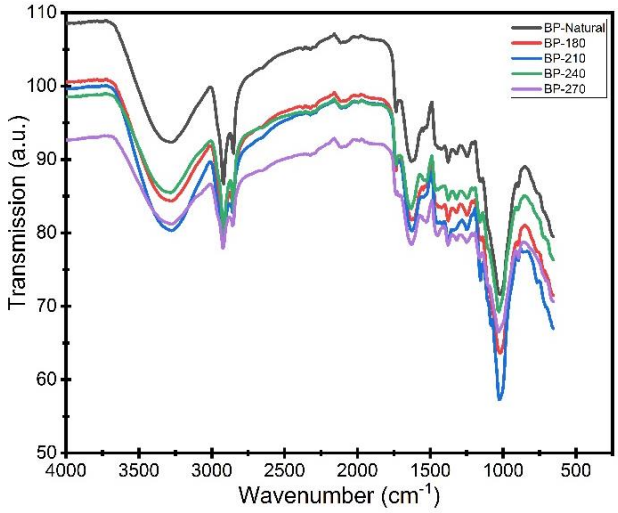

Fig. 5. Comparison of FTIR results from BP-180, BP-210, BP-240, and BP-270.

2. FTIR Results

The FTIR spectrum BP-180, BP-210, BP-240, and BP-270 are shown in the following Figure 4. The wide band centered at about 3440 cm^{-1} corresponds to the O–H stretch vibration of the hydroxyl alcohol group, the wide band at about 1620 cm^{-1} can be attributed to the C=O stretch vibration of the carboxylate and aldehyde groups, the peak at 1450 cm^{-1} corresponds to the O–H stretch vibration of the phenol hydroxyl group, the peak at 1110 cm^{-1} indicates the CO stretch vibration of the alcohol or phenol, and the peak at 883 cm^{-1} is the vibrational of the aromatic C–H curving out of the field. After the temperature increase, the peak stretch vibration at 3440 cm^{-1}, 1620 cm^{-1}, 1450 cm^{-1}, and 1110 cm^{-1} for BP-210, BP-240, and BP-270 increased compared to BP-180 due to the formation of alcohols, phenols, and other substances containing CO bonds or further oxidation into ketones, aldehydes, and carboxylic acids containing C=O bonds during electrolysis. Furthermore the peak of the C–H bond becomes larger at 883 cm^{-1}, which indicates that more aromatic carbon is produced during the banana peel temperature increase [8].

3. UV-Vis with Tauc's Relation Results

According to optical and electronic analysis, the catalyst photoactivity regulated by the effective separation of the charge carrier and the charge transfer of the interface is closely related to the edge level of the semiconductor band. The determination of the energy gap and valence band edge between the (valence band) VB and the (conduction band) of the CB electrolyte catalyst was tested based on UV-Vis light absorption and then converted using the Tauc's Relation as shown in Figure 5 and Eq. (1) [18].

$$\alpha h v = A(hv - E_g)^{\frac{n}{2}} \quad (1)$$

Where α is the absorption coefficient of the semiconductor represented by, hν is the energy of the photon, and A is the constant. The value of n depends on the type of semiconductor optical transition (n = 1 for direct transition and n = 4 for indirect transition) [19]. Based on Pearson's absolute electronegativity, the absolute electronegativities of C, O, Si, and K are 6.27 eV, 7.54 eV, 4.77 eV, and 2.42 eV, respectively [20]. Meanwhile, the number of atoms included in the calculation of determining the value of X is obtained from the results of the presentation of atoms from EDX. Thus, the X calculated for Banana Peel is 5.89 eV. The electronegativity value obtained is determined (shown in Figure 5(b)) and then paired in the Eq. (2), (3), and (4).

$$E_{VB} = X - E^e + 0.5E_g \quad (2)$$

$$E_{CB} = E_{VB} - E_g \quad (3)$$

$$X(AmBnCl) = \sqrt[(m+n+l)]{X_A^m\, X_B^n\, X_C^l} \quad (4)$$

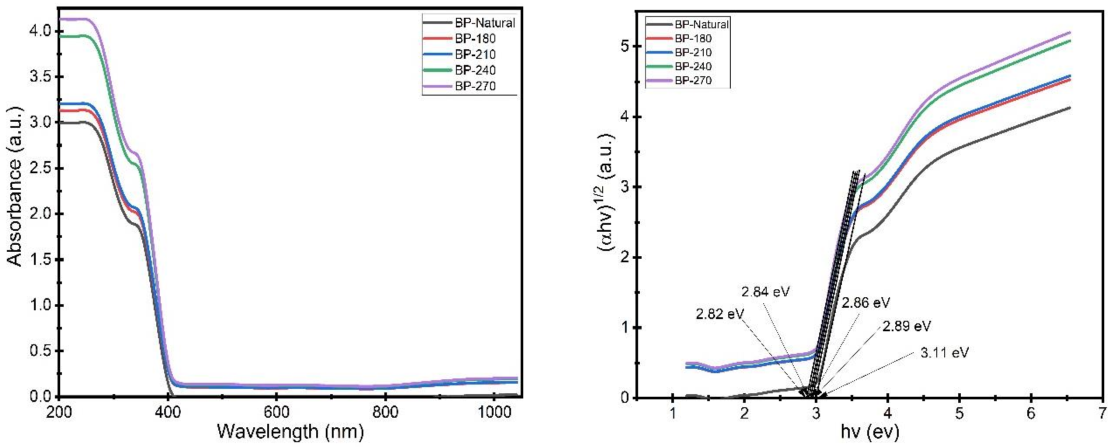

(a) **(b)**

Fig. 6. (a) UV-Vis test results, (b) Tauc's relation results.

4. *Photocatalytic Mechanism*

The energy bandgap and valence band edge values can be calculated based on the UV-Vis result, the percentage of EDX results, and Tauc's Relation, as seen in Figure 6. The activation mechanism of temperature increase in banana peel biochar can be concluded by integrating the results of SEM-EDX, FTIR, UV-Vis, and TGA characterization. First, the free hydroxide (OH−) ions in solution release electrons and are oxidized into highly reactive oxygen radicals (·OH). Then, ·OH oxidizes the active sites in the banana peel biochar, including aliphatic C–H, C–OH, and C=O, into C–OH, C=O, and COOH. The reaction path is shown in Eq. (5)-(8).

$$OH^- + \cdot \rightarrow \cdot OH + e^- \quad (5)$$

$$C - H + \cdot OH \rightarrow C - OH + H_2O \quad (6)$$

$$C - OH + \cdot OH \rightarrow C = O + H_2O \quad (7)$$

$$C = O + \cdot OH \rightarrow COOH \quad (8)$$

The mechanism of the photocatalytic process on the surface is explained in Figure 7, quoted from the book Photocatalysis-Fundamentals [21]. Hydroxide ions are one of the molecules on the oxide surface formed on banana peel. The oxides formed include alcohol, phenol, and carboxylic acid. The presence of these oxides is evident in the results of FTIR testing, coupled with the presence of aromatic groups. Oxides on the surface function to interfere with the breaking of hydrogen bonds in H_2O if the accumulation of electrons accumulates in this phase [22]. Electrons will tend to accumulate, and the energy value will be greater than the Gibbs energy [23]. As a result, the electrons will leave a positively charged hole and attract oxygen to the covalent bond in H_2O. The greater the oxidation energy (more significant than the Gibbs Energy), the greater the likelihood that the hydrogen bond to the covalent bond in H_2O will break [24]. The biochar surface activation mechanism validated the banana peel biochar deformation by accumulating the entire Surface of pores. The pores on the Surface were validated using the SEM and 3D Surface results using the ImageJ application. Thermogravimetric testing showed an increase in temperature, which decreased the weight percentage of banana peel biochar, as seen in Figure 8. The increase in the number of pores was validated through the ImageJ application threshold tool on the SEM image results.

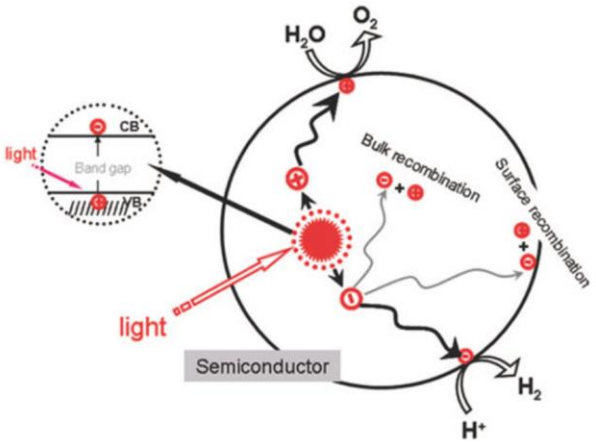

Fig. 7. Mechanism of hydrogen production from photocatalytic process [21].

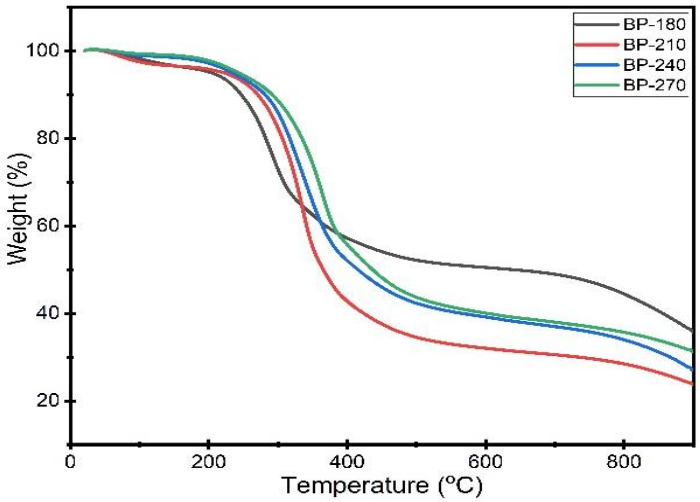

Fig. 8. TGA test results.

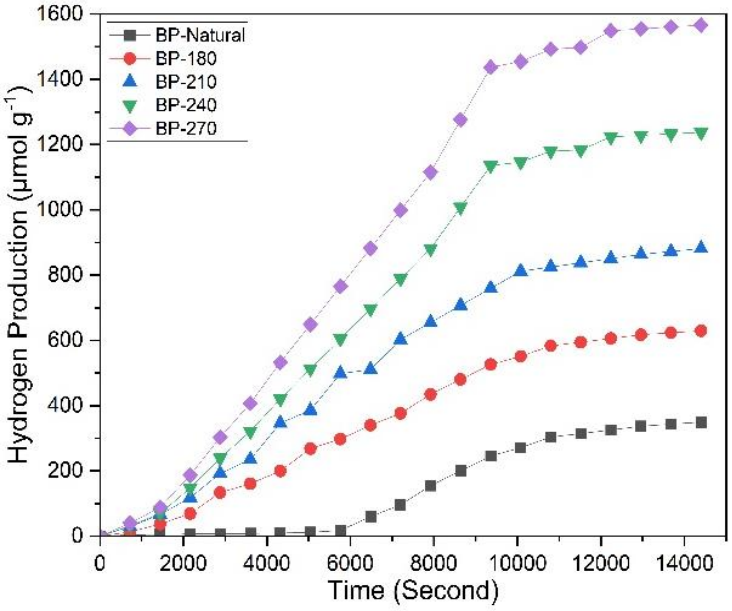

Fig. 9. Hydrogen production test results.

5. Hydrogen Production with TGA Effect on Surface Pore

The TGA results in Figure 8, show that all variations of Banana Peel are able to maintain the most stable weight percentage, at 94% at a temperature of 293ºC. The data is compared to the percentage of weight loss at a temperature of 400ºC. In general, the degradation of the weight percentage in banana peel is up to a temperature of 900ºC. This value shows that the greatest energy is needed, which is 1709190.45 Joules or equivalent to 1.0667 x 10^{25} eV. At the same time, the energy provided by UV-A is 3.099 eV, which is equivalent to 2.6149 x 10^{-22} ºC or 4.9661 x 10^{-19} Joule. Based on the average pores formed by the method used in this study, it explains that the temperature at BP-270 has been able to provide performance in hydrogen production in the UV-A exotherm. So there needs to be further research with temperatures approaching the range of 800ºC - 900ºC.

The results of hydrogen production in double chamber photoelectrochemistry with UV-A irradiation are shown in Figure 9. Hydrogen production of BP-270 sequentially has the highest value of 1566.05 µmol·g^{-1} compared to BP-240, BP-210, and BP-180. Hydrogen production in BP-240, BP-210, BP-180, and BP-Natural decreased hydrogen production by 1219 µmol·g^{-1}, 881.7 µmol·g^{-1}, 629.41 µmol·g^{-1}, and 297 µmol·g^{-1}, respectively. Based on light absorbance, the UV-Vis test results showed that the wavelength of BP-270 was closer to the UV-A range, which was 439.66 nm, while the wavelengths of BP-240, BP-210, and BP-180 were 436.56 nm, 433.51 nm, and 429.01 nm, respectively. The proximity of the absorbance level to the wavelength of light can maximize oxidation at the ValenceBand position. This explains that exothermic energy can activate endothermic energy in BP for oxidation efficiency. However, when heat treatment can grow more pores on the surface, the pores on the surface can increase light absorption and facilitate the separation of photogenerated charge carriers. Strong oxidation maintains the conditions for forming holes (h^+) and electrons (e^-) so that the BP surface is facilitated in receiving electrons. The tragedy is validated from the perspective of the energy bandgap, which is calculated from the UV-Vis results with Tauc's Relation approach. It can be seen that BP-270, BP-240, BP-210, BP-180, and BP-Natural each produce an energy bandgap of 2.82 eV, 2.84 eV, 2.86 eV, 2.89 eV and 3.11. The gap value between one and another shows that increasing temperature decreases the bandgap distance. The closeness of the energy bandgap distance makes the

electron jump time from the valence band to the conduction band faster. This makes the holes on the surface faster to oxidize H_2O in the vicinity for the production of O_2 and electrons faster to reduce H_2O for the production of H_2. Based on a comparison of previous studies, the dual photoelectrochemical chamber can produce hydrogen from a banana peel photocatalyst at 1219 $\mu mol \cdot g^{-1}$ (see Table 2).

Table 2. Results and summary with previous studies.

Ref	Photocatalyst	Source	Hydrogen Production
[25]	Coconut shell carbon nanosheets (CSC)	300 W xenon lamp	1679.5 $mmol \cdot g^{-1} \cdot h^{-1}$
[26]	Ti-PH + L-cys	UV Lamp	150 $\mu mol \cdot g^{-1}$
[9]	CBW	400 W high pressure mercury lamp	575 $\mu mol \cdot g^{-1} \cdot h^{-1}$
[16]	Zn/ZnO + BBN + BT	500-W halogen lamp	2784 $\mu mol \cdot g^{-1}$
[14]	Coffee waste	500-W halogen lamp + External magnetic field	38956 $\mu mol \cdot g^{-1}$
[7]	ZnO + carbon banana Peel	150-W solar lamp	1846.4 $\mu mol \cdot g^{-1} \cdot h^{-1}$
This Study	BP-270	15-W UV-A lamp	391.5125 $\mu mol \cdot g^{-1} \cdot h^{-1}$
	BP-240		304.75 $\mu mol \cdot g^{-1} \cdot h^{-1}$
	BP-210		220.425 $\mu mol \cdot g^{-1} \cdot h^{-1}$
	BP-180		157.3525 $\mu mol \cdot g^{-1} \cdot h^{-1}$
	BP-Natural		74.25 $\mu mol \cdot g^{-1} \cdot h^{-1}$

IV. Conclusions

The formation of pores on the BP surface successfully increased along with the increase in temperature of 30 ^oC, 180 ^oC, 210 ^oC, 240 ^oC, and 270 ^oC. The surface of BP-270 has more pores than BP-240, BP-210, BP-180, and BP-Natural. The pores are proven by the surface morphology of SEM results and weight loss through thermogravimetric tests. Forming a narrow energy band in line with the UV-A wavelength range value approach can produce optimal hydrogen production. BP-270 can produce the most significant hydrogen of 1566.05 $\mu mol \cdot g^{-1}$, compared to BP-240, BP-210, and BP-180. Conclusively, this study provides a promising approach for developing photoelectrochemical and finding and eliminating organic waste for hydrogen-producing materials.

Acknowledgment

This research is provided by the Faculty of Engineering, Pancasila University, under the Fundamental Research Group Grant Program 2024. The authors would like to thank the Advanced Energy Conversion Laboratory, Pancasila University.

References

[1] L. Clarizia, M.N. Nadagouda, and D.D. Dionysiou, "Recent advances and challenges of photoelectrochemical cells for hydrogen production," *Curr Opin Green Sustain Chem*, vol. 41, Jun. 2023, doi: 10.1016/j.cogsc.2023.100825.

[2] F. Tavasol, T. Tabatabaie, B. Ramavandi, and F. Amiri, "Design a new photocatalyst of sea sediment/titanate to remove cephalexin antibiotic from aqueous media in the presence of sonication/ultraviolet/hydrogen peroxide: Pathway and mechanism for

degradation," *Ultrason Sonochem*, vol. 65, no. February, p. 105062, 2020, doi: 10.1016/j.ultsonch.2020.105062.

[3] L. Chen, B. Mi, J. He, Y. Li, Z. Zhou, and F. Wu, "Functionalized biochars with highly-efficient malachite green adsorption property produced from banana peels via microwave-assisted pyrolysis," *Bioresour Technol*, vol. 376, no. February, p. 128840, 2023, doi: 10.1016/j.biortech.2023.128840.

[4] K. Pandey and H.K. Jeong, "Coffee waste-derived porous carbon for hydrogen and oxygen evolution reaction," *Chem Phys Lett*, vol. 6, Jun. 2022, doi: 10.1016/j.chphi.2023.100175.

[5] W.M. Hikal, H.A.H.S. Al Ahl, A. Bratovcic, K.G. Tkachenko, J. Sharifi-Rad, M. Kačániová et al., "Banana peels: A waste treasure for human being," *Evidence-based Complementary and Alternative Medicine*, vol. 2022, no. May, p.7616452, 2022, doi: 10.1155/2022/7616452.

[6] M. Razali, J. Sembiring, and M. Taufik, "Bioactive compounds in barangan banana peel (Musa acuminata Colla.) as an alternative for antibacterial drug development," *Journal of Carbazon*, vol. 1, no. 2, pp. 12–17, 2023, doi: 10.24815/jocarbazon.v2i1.36402.

[7] H. Abdullah, R.T. Ginting, H. Shuwanto, and D.H. Kuo, "Banana peel biowaste-derived carbon composited with Zn(O,S) for solar-light photocatalytic hydrogen generation," *Int J Hydrogen Energy*, vol. 47, no. 97, pp. 41021–41033, 2022, doi: 10.1016/j.ijhydene.2022.09.184.

[8] D. Sartika, D. Widhiyanuriyawan, A.S. Widodo, Purnami, and I.N.G. Wardana, "The role of graphene oxide's aromatic rings in activated carbon made from banana leaves (ACBL) and Fe3O4 in hydrogen production," *Carbon Resources Conversion*, no. April, p. 100239, 2024, doi: 10.1016/j.crcon.2024.100239.

[9] S.M. Unni, L. George, S.N. Bhange, R.N. Devi, and S. Kurungot, "Valorization of coffee bean waste: A coffee bean waste derived multifunctional catalyst for photocatalytic hydrogen production and electrocatalytic oxygen reduction reactions," *RSC Adv*, vol. 6, no. 85, pp. 82103–82111, 2016, doi: 10.1039/c6ra14907c.

[10] N.W. Satrio, Winarto, Sugiono, and I.N.G. Wardana, "Hydrogen production from instant noodle wastewater by organic electrocatalyst coated on PVC surface," *Int J Hydrogen Energy*, vol. 45, no. 23, pp. 12859–12873, 2020, doi: 10.1016/j.ijhydene.2020.03.002.

[11] L. Sivasankaran, S.C. Pradhan, R.K. Mishra, S. Soman, and A. Ajayaghosh, "Role of alkyl groups regulating recombination and mass transport at cobalt electrolyte-dye interface in dye sensitized solar cells," *Solar Energy*, vol. 236, no. March, pp. 182–194, 2022, doi: 10.1016/j.solener.2022.03.001.

[12] Y.K. Sofi'i, E. Siswanto, Winarto, T. Ueda, and I.N.G. Wardana, "The role of activated carbon in boosting the activity of clitoria ternatea powder photocatalyst for hydrogen production," *Int J Hydrogen Energy*, vol. 45, no. 43, pp. 22613–22628, 2020, doi: 10.1016/j.ijhydene.2020.05.103.

[13] D. Dai, Y. Li, and J. Fan, "Room-temperature synthesis of various allotropes of carbon nanostructures (graphene, graphene polyhedra, carbon nanotubes and nano-onions, n-diamond nanocrystals) with aid of ultrasonic shock using ethanol and potassium hydroxide," *Carbon*, vol. 179, pp. 133–141, 2021, doi: 10.1016/j.carbon.2021.04.038.

[14] A.F. Alphanoda, E. Prasetyo, and W. Broto, "Photocatalytic scheme with external magnetic field on coffee waste in hydrogen production," *Journal of Mechanical Engineering Science and Technology (JMEST)*, vol. 7, no. 2, pp. 181-189, 2023, doi: 10.17977/um016v7i22023p181.

[15] M.S. Santana, R.P. Alves, L.S. Santana, M.A. Gonçalves, and M.C. Guerreiro, "Structural, inorganic, and adsorptive properties of hydrochars obtained by hydrothermal carbonization of coffee waste," *J Environ Manage*, vol. 302, Jan. 2022, doi: 10.1016/j.jenvman.2021.114021.

[16] A.F. Alphanoda, Winarto, F. Gapsari, W.S. Nugroho, and I. Wardana, "Multi-output photoelectrochemical system based on Zn / ZnO using aqueous bismuth tea waste electrolyte to produce hydrogen and electricity," *Int J Hydrogen Energy*, vol. 67, pp. 1117-1135, 2024, doi: 10.1016/j.ijhydene.2023.09.303.

[17] D. Wu, Y. Shi, H. Jing, X.Wang, X.Song, D. Si et al., "Tea-leaf-residual derived electrocatalyst: Hierarchical pore structure and self nitrogen and fluorine co-doping for efficient oxygen reduction reaction," *Int J Hydrogen Energy*, vol. 43, no. 42, pp. 19492–19499, 2018, doi: 10.1016/j.ijhydene.2018.08.201.

[18] P.R. Jubu, O.S. Obaseki, A. Nathan-Abutu, F.K. Yam, Y. Yusof, and M.B. Ochang, "Dispensability of the conventional Tauc's plot for accurate bandgap determination from UV–vis optical diffuse reflectance data," *Results in Optics*, vol. 9, p.100273, Dec. 2022, doi: 10.1016/j.rio.2022.100273.

[19] M. Junaid, Noor-ul-ain, and W.Q. Khan, "Bandgap alignment of solar-driven multilayers metal oxide thin film for water splitting to generate hydrogen energy," *Int J Hydrogen Energy*, vol. 52, pp. 199-208, 2024, doi: 10.1016/j.ijhydene.2023.06.161.

[20] R.G. Pearson, "Absolute Electronegativity and Hardness: Application to Inorganic Chemistry," *Inorg. Chem*, vol. 27, pp. 734–740, 1988, Accessed: Jul. 04, 2023. [Online]. Available: https://doi.org/10.1021/ic00277a030

[21] J. Zhang, B. Tian, L. Wang, M. Xing, and J. Lei, *Photocatalysis-Fundamentals, Materials and Applications*. Singapore: Springer Nature Singapore, 2018. doi: 10.1007/978-981-13-2113-9.

[22] M. Remko and J. Polcin, "Theoretical study of the hydrogen bonding ability of phenol and its ortho, meta and para substituted derivatives," *Advances in Molecular Relaxation and Interaction Processes*, vol. 11, no. 3–4, pp. 249–254, 1977, doi: 10.1016/0378-4487(77)80037-X.

[23] Z. Xie, G. Liu, L. Xie, P. Wu, H. Liu, J. Wang et al., "Promoting photocatalytic H2 evolution through interfacial charge separation on the direct Z-scheme ZnIn2S4/ZrO2 heterojunction," *Int J Hydrogen Energy*, vol. 84, no. 84, pp. 32782-32796, 2023, doi: 10.1016/j.ijhydene.2023.05.038.

[24] Purnami, N. Hamidi, M.N. Sasongko, D. Widhiyanuriyawan, and I.N.G. Wardana, "Strengthening external magnetic fields with activated carbon graphene for increasing hydrogen production in water electrolysis," *Int J Hydrogen Energy*, vol. 45, no. 38, pp. 19370–19380, 2020, doi: 10.1016/j.ijhydene.2020.05.148.

[25] D.W. Zha, L.F. Li, Y.X. Pan, and J.B. He, "Coconut shell carbon nanosheets facilitating electron transfer for highly efficient visible-light-driven photocatalytic hydrogen production from water," *Int J Hydrogen Energy*, vol. 41, no. 39, pp. 17370–17379, 2016, doi: 10.1016/j.ijhydene.2016.07.227.

[26] H. Pan, W. Liao, N. Sun, M. Murugananthan, and Y. Zhang, "Highly efficient and visible light responsive heterojunction composites as dual photoelectrodes for photocatalytic fuel cell," *Catalysts*, vol. 8, no. 1, Jan. 2018, doi: 10.3390/catal8010030.